REPORT DOCUMENTATION PAGE

PLEASE DO NOT RETURN YOUR FORM TO THE ABOVE ORGANIZATION.

1. REPORT DATE	2. REPORT TYPE	3. DATES COVERED	
		START DATE	END DATE
20220103	Conference Paper	20211201	20220131

4. TITLE AND SUBTITLE

Wave Structure of Heterogeneous Detonations in Rotating Detonation Rocket Engines

5a. CONTRACT NUMBER	5b. GRANT NUMBER	5c. PROGRAM ELEMENT NUMBER
5d. PROJECT NUMBER	**5e. TASK NUMBER**	**5f. WORK UNIT NUMBER**
		Q2B5

6. AUTHOR(S)

Ariana Martinez, Stephen Heister

7. PERFORMING ORGANIZATION NAME(S) AND ADDRESS(ES)

Air Force Research Laboratory (AFMC)
AFRL/RQRC
10 E. SATURN BLVD,
EDWARDS AFB, CA 93524-7680

8. PERFORMING ORGANIZATION REPORT NUMBER

9. SPONSORING/MONITORING AGENCY NAME(S) AND ADDRESS(ES)	10. SPONSOR/MONITOR'S ACRONYM(S)	11. SPONSOR/MONITOR'S REPORT NUMBER(S)
Air Force Research Laboratory (AFMC), AFRL/RQR 5 Pollux Drive Edwards AFB, CA 93524-7048		AFRL-RQ-ED-TP-2021-312

12. DISTRIBUTION/AVAILABILITY STATEMENT

Distribution Statement A: Approved for Public Release; Distribution is Unlimited. PA Clearance Number: AFRL-2021-4305
Clearance Date: 06 Dec 2021

13. SUPPLEMENTARY NOTES

For presentation at AIAA 2022 SciTech Forum January 3-7,2022; San Diego,CA
The U.S. Government is joint author of the work and has the right to use, modify, reproduce, release, perform, display, or disclose the work.
Prepared in collaboration with Purdue University

14. ABSTRACT

A strong motivation exists to better understand the wave structure of heterogeneous detonations, as rotating detonation rocket engines (RDREs) are best-suited for engine cycles employing gas/liquid propellants. Experimental studies to examine the wave structure of heterogeneous detonations have only been conducted in detonation tubes at base pressures of 1 atmosphere or less, with all of these studies dating back several decades.

15. SUBJECT TERMS

16. SECURITY CLASSIFICATION OF:			17. LIMITATION OF ABSTRACT	18. NUMBER OF PAGES
a. REPORT	b. ABSTRACT	C. THIS PAGE		
Unclassified	Unclassified	Unclassified	SAR	18

19a. NAME OF RESPONSIBLE PERSON	19b. PHONE NUMBER *(Include area code)*
John Bennewitz	N/A

PREVIOUS EDITION IS OBSOLETE.

STANDARD FORM 298 (REV. 5/2020)
Prescribed by ANSI Std. Z39.18

Wave Structure of Heterogeneous Detonations in Rotating Detonation Rocket Engines

Ariana Martinez* and Stephen Heister†
Purdue University, West Lafayette, IN, 47907

A strong motivation exists to better understand the wave structure of heterogeneous detonations, as rotating detonation rocket engines (RDREs) are best-suited for engine cycles employing gas/liquid propellants. Experimental studies to examine the wave structure of heterogeneous detonations have only been conducted in detonation tubes at base pressures of 1 atmosphere or less, with all of these studies dating back several decades. In this manuscript, we identify key factors that influence the wave dynamics of heterogeneous detonations, and have constructed a simple model to inform the behavior of a droplet in a heterogeneous detonation flowfield. The purpose of this model is do discern trends in the time and length of the reaction zone as droplet size, base pressures, and mixtures are varied. The analysis focuses on the behavior of the droplet, and utilizes an analysis to estimate the rate of mass shed off the droplet based on viscous boundary layer instabilities at the free surface of the gas/liquid interface. The trajectory of the droplet is computed by assuming that it travels through gas medium that matches a ZND profile. It is found that the droplet size and the dynamic pressure induced onto the droplet by the leading shock front are the two most important factors that affect the droplet breakup process. It is found that smaller droplet diameters, higher base pressures, and reactants with lower sound speeds are desired for close coupling of the leading shock front to the heat-release zone. The model results are applied to a gox/kerosene RDRE test with known injector sizing and wavespeed, and it is found that there may be short bursts of discrete, intense heat release followed by substantial periods of little heat release in between adjacent injector elements. The implications of this detonation wave structure are discussed.

I. Nomenclature

D	=	droplet diameter
k_r	=	length scaling factor
k_t	=	time scaling factor
m	=	droplet mass
$\bar{m}$	=	nondimensionalized droplet mass, $\frac{m}{m_0}$
P	=	static pressure
q	=	dynamic pressure
t^*	=	characteristic time
t	=	dimensional time
T	=	temperature
u	=	lab frame velocity
We	=	weber number
α	=	ratio of gas density to liquid density
β	=	ratio of gas dynamic viscosity to liquid dynamic viscosity
ϕ_{gl}	=	global equivalence ratio
ϕ_{eff}	=	effective equivalence ratio
μ	=	dynamic viscosity
ρ	=	density
σ	=	surface tension
τ	=	nondimensional time

*Graduate Research Assistant, School of Aeronautics and Astronautics,701 W Stadium Ave, IN, and AIAA Student Member
†Raisbeck Distinguished Professor, Department of Aeronautics and Astronautics, 701 W Stadium Ave, IN, and AIAA Fellow.

subscripts

0 = initial conditions, prior to passage of the leading shock front
2 = conditions immediately behind the leading shock front
g = gas properties
l = liquid properties
b = contitions at time of droplet breakup

Introduction

As the propulsion industry continues to move towards pressure gain combustion as a viable concept, understanding the complex nature of heterogeneous detonations is becoming increasing essential as rocket detonation engines will need to utilize gas/liquid systems in order to be competitive with the highly efficient systems of today's market. The goal of this work is to better understand detonation behavior for applications to gas/liquid rotating detonation rocket engines (RDREs) by highlighting the key processes that influence the wave dynamics of heterogeneous detonations. A detailed literature review of experimental studies of heterogeneous detonations has been conducted by Humble and Heister [1], and this review reveals that the detailed process of droplet shattering in detonation waves relies on complex flow phenomena, including atomization and gas-liquid droplet interaction, phase mass transfer, local sound speed variation due to two-phase media, and transcritical behavior. In and effort to bypass these challenges in modelling the droplet behavior, the current work focuses on modeling the droplet shattering process using empirical correlations from experimental data in literature.

Much early work [2–5] done to illuminate the droplet shattering process behind shocks was done for the purpose of investigating rain erosion on high-speed vehicles. Engel [2] Investigated the fragmentation of 1.4-2.7 mm water droplets exposed to Mach 1.5 and 1.7 shocks in air. Nicholson and Hill [3] then increased the range of Mach numbers to Mach 3 and decreased the base pressure for simulated altitude. Reinecke and Mcay [4] then increased shock Mach up to Mach 11 at simulated altitude and studied the breakup characteristics of 1 mm water droplets. Reinceck and Waldman [4] then used the same test conditions, but doped the water droplets to study the effect of increasing the droplet density. In each of these works, the drop displacement, droplet shattering time, and computed drag coefficient were reported and are summarized in Table 1.

Table 1 Experimental results of liquid droplet interactions with shocks and detonation waves

Author	Shock Mach	P_0 (atm)	$D_0(\mu m)$	Mixture	x_d (mm)	t_b (μs)	C_d	q_2 (atm)
Engel [2]	1.50 & 1.70	1.0	1400 & 2700	H_2O/Air	12-29	452 - 764	0.25	0.63 & 1.32
Nicholson & Hill [3]	1.81-2.93	0.07 - 0.41	1800	H_2O/Air	22	305-990	2.67	0.19-2.41
Ragland et al. [6]	3.09	1.0	2600	DECH/O_2	65	450	1.5	15
Reinecke & Mcay [4]	2.51 - 11.4	0.6	1000	H_2O/Air	12 - 29	18 - 202	2.13	4.3 - 215
Daborah et al. [7]	5.07 & 3.23	1.0	290 & 2600	DECH/O_2	127	20 & 550	-	17 & 59
Nicholls & Ranger [8]	1.5 - 3.51	1.0	900 - 2700	H_2O/Air	35-116	95-831	3	0.63-22
Reinecke & Waldman [5]	3.00 - 11.0	0.18 - 1.0	2120	Doped H_2O/Air	2 - 16	25 - 150	2.13	13 - 60
Kauffman & Nicholls * [9]	2.4 - 4.78	0.33 - 1.0	933 & 1520	DECH/N_2	-	35 - 209	-	4.1 - 33
Kauffman & Nicholls† [9]	2.78 - 4.70	0.33 - 1.0	933 & 1520	DECH/O_2	-	47 - 153	-	6.9 - 32
Boiko et al. [10]	2.37 - 3.80	0.28 & 1.0	700 - 3200	H_2O/ He‡	0.13 - 182	110 - 320	2.3	5.5 - 7.4

Cramer [11] utilized $O_2(g)/DECH$ mixtures in a self-propagating detonation wave in a heterogeneous flow field. The flattening and breakup of fuel droplets was observed, and this work led to the important conclusion that microdrops shed from the parent drop must be approximately 10 microns or smaller in order to sustain the detonation wave. This conclusion was supported by Bowen [12], who studied the heterogeneous detonation behavior of 2 micron droplet "fogs", and found that the wave propagation velocity approaches the ideal gas/gas CJ velocity as the droplet size gets smaller.

*nonreacting flow
†reacting flow
‡Glycerine and tridecane also tested

Dabora, Ragland, and Nicholls [6, 13] studied monodisperse 940 and 2600 micron DECH drops in O_2, and determined that the gasdynamic properties behind the leading shock front of a heterogeneous detonation could be approximated through 1-D shock-jump conditions, consistent with an ideal ZND model. They also concluded that droplet shattering is a rate-controlling mechanism of combustion behind a heterogeneous detonation wave.

Daborah et al. [7] investigated the effect of drop size on heterogeneous detonation wave behavior in more depth, studying 290, 940, and 2600 micron DECH drops in O_2. They show that detonation wave velocity increases with decreasing droplet diameter due to a longer reaction zone length controlled by the droplet breakup process. The exception to this is with high vapor pressure droplets, which were studied by Bar-Or et al. [14, 15]. It was found that while the reaction zone length was governed by droplet breakup for low vapor pressure fuels, the reaction-zone length for high vapor pressure fuels was much shorter due to the large amount of gaseous fuel already present.

Kauffman and Nicholls [9] demonstrated experimentally that liquid fuel droplets in an oxygen environment could be autoignited by the presence of a shock wave, and studied the difference in droplet breakup time between reacting and nonreacting flows. They discovered a minor decrease in droplet breakup time for reacting flows, but ultimately determined that the most important factor affecting droplet breakup time is the dynamic pressure behind the leading shock front, q_2, where the droplet breakup time scales inversely with the square root of q_2.

A. Droplet Shattering Times in Literature

Droplet breakup data has been compiled [2–10] has been compiled and studied for trends. It was found that the most compelling and consistent trend among various literature sources is that proposed by Kauffman and Nicholls [9], where the droplet breakup time scales inversely with $\sqrt{q_2}$. The compiled data is shown in Fig. 1.

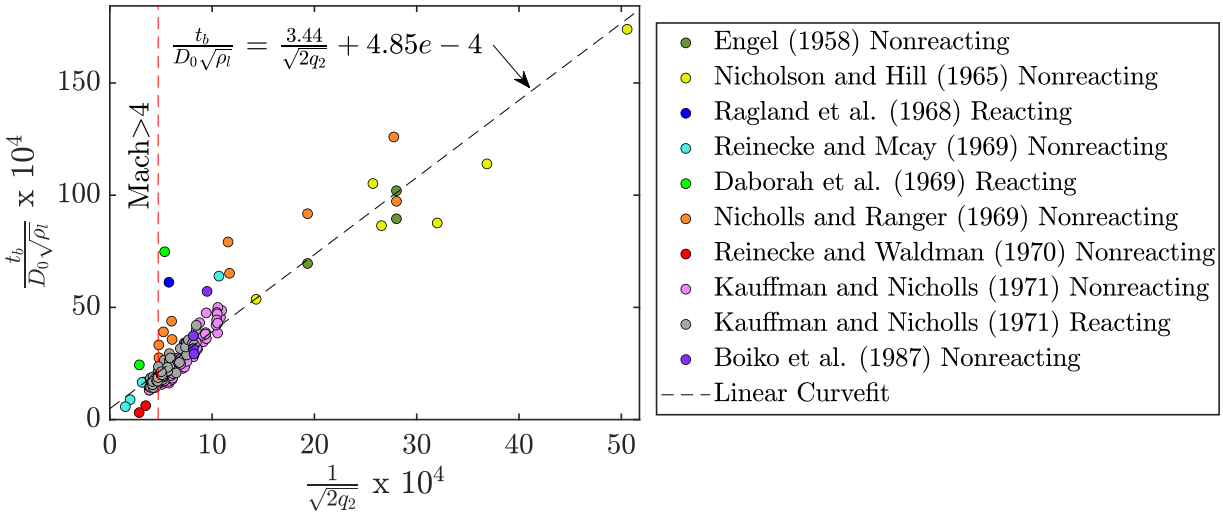

Fig. 1 Compiled experimental data from literature showing reported droplet breakup time as a function of the dynamic pressure behind the leading shock front. t_b is droplet breakup time in s, D_0 is initial droplet diameter in m, ρ_l is liquid density in kg/m^3, and q_2 is the gas dynamic pressure immediately behind the leading shock front, in Pa.

The droplet breakup time can be nondimensionalized by the characteristic time, t^*, which is the characteristic time associated with deforming the drop on the order of the original droplet diameter, D_0 [5]. Characteristic time is given by Eq. (1):

$$t^* = \frac{D_0}{u_{2g}}\sqrt{\frac{\rho_l}{\rho_{2g}}} = \frac{D_0\sqrt{\rho_l}}{\sqrt{2q_2}} \tag{1}$$

Where u_2 is the lab frame gas velocity behind the leading shock front and ρ_l is the liquid droplet density. Thus, the nondimensional breakup time, T_b, is given by:

$$\tau_b = \frac{t_b}{t^*} = \frac{t_b\sqrt{2q_2}}{D_0\sqrt{\rho_l}} \tag{2}$$

Where t_b is the dimentional breakup time in seconds. Thus, plotting $\frac{t_b}{D_0\sqrt{\rho_l}}$ vs $\frac{1}{\sqrt{2q_2}}$ in Fig. 1 collapses the data to an approximately linear trend, where the slope of this linear trendline closely follows the nondimensional breakup time. T_b is determined from the compiled data to be:

$$\tau_b = 3.44 + 4.85 * 10^{-4}\sqrt{2q_2} \tag{3}$$

In analyzing droplet shattering data that spans both reacting and nonreacting flows over a range of liquid and gas mediums, the authors argue that the only significant factors effecting droplet breakup time in a detonation wave are (1) the size of the droplet and (2) the dynamic pressure that the droplet experiences. Liquid density is a factor that affects how rapidly the droplet can deform. However, from a practical sense, liquid densities being considered for RDRE applications will vary by less than an order of magnitude and is thus not as impactful of a parameter as droplet size and dynamic pressure.

The authors argue that surface tension forces, and thus Weber number, become irrelevant parameters because surface tension forces are negligible compared to the dynamic pressure acting on the droplet. To demonstrate this, consider a stationary 900 μm water droplet being hit by a Mach 3 shock wave in air at ambient base pressure, as was in the experimental data of [8]. From normal shock relations, the relative velocity between the air and the droplet immediately after the shock passage is 773 m/s, putting the dynamic pressure experienced by the drop to be 13.5 atm. If we assume the droplet surface tension to be that of a water droplet in ambient pressure and temperature, the surface tension of the water droplet is .073 N/m. This puts the weber number at 3.4E4, where Weber number, We, is computed by Eq. (4). Stated another way, the forces acting to break the droplet apart are 4 orders of magnitude greater than the forces acting to hold the droplet together.

$$We = \frac{\rho_g u_g^2 D_0}{\sigma} = \frac{2qD_0}{\sigma} \tag{4}$$

Thus, we may conclude that surface tension is not a relevant parameter affecting the droplet breakup process in heterogeneous detonations. Furthermore, it may be inferred from this conclusion that subcritical, transcritical, and supercritical droplets will exhibit similar trends in droplet shattering behavior.

B. Mass Loss Models in Literature

While droplet breakup times have been well documented in literature, The rate of mass loss from the droplet has not been well documented, as this metric is difficult to measure experimentally. In numerical studies [16], droplet vaporization models with forced convection have been utilized. Eidelman and Burcat [17] utilized a hybrid shattering/vaporization model, and Borisov [18] compared a droplet shattering model to a vaporization model, finding that the droplet shattering model better reproduced experimental data.

Although vaporization models may be appropriate in detonation waves with lower propagation velocities, conditions relevant to RDREs involve leading shock fronts in excess of Mach 4, where droplet breakup times are likely less than 100 μs, and elevated base pressures (at least 10 atm), where pressures and temperatures behind the shock will push the droplet into the supercritical range. Because of the short timescales and transcritical nature associated with the conditions of interest, it is concluded that droplet vaporization models would be inaccurate in capturing the physics of liquid dispersion into the gas [19]. It is instead asserted that the rate of mass loss from the droplet is dominated by the mechanical shearing exerted by the gas onto the liquid surface to form a boundary layer.

A boundary-layer stripping model was proposed by proposed by Nicholls & Ranger [8]. In this model, the rate of mass loss off the parent droplet is estimated by determining the thickness of the liquid boundary layer and integrating over the surface of the drop to determine the mass flux. It is assumed that the mass of liquid in the boundary layer is the mass that is stripped from the droplet. Although this analysis is elegant in that shear stripping only requires the density and viscosity to be relevant fluid properties, it requires the assumption of incompressible gas flow. Thus, as has been previously noted in literature, [5] this approach will significantly underpredict the rate of mass stripping at higher dynamic pressures.

We instead use the analysis proposed by Girin [20, 21], in which an analysis separate from a boundary-layer analysis or a rayleigh-taylor analysis is conducted. This model proposes that hydrodynamic instabilities form on the surface of a droplet in high-speed gas flow due to the large gradient of inertial forces caused by the velocity difference. this analytical approach is the most suitable for investigating droplet mass loss in heterogeneous detonations because it captures that the dynamic pressure acting on the droplet is the single most important factor effecting the breakup process. The timescale of the process is the time scale associated with the development time of an unstable wave on the fluid

boundary, and the mass loss is associated with the length of unstable waves. The resulting equation obtained for the rate of nondimensionalized mass loss of a droplet, $\frac{m}{m_0}$, is given in Eq. 5.

$$\frac{d\bar{m}}{dT} = -A\bar{m}(T)^{2/3}\left(1 - \frac{u_l(T)}{u_{2g}}\right) \tag{5}$$

$$A \equiv 0.405\frac{\pi^3 k_r^2}{k_t\left(1+\alpha^{\xi}\right)}\alpha^{1/6}\beta^{1/3} \tag{6}$$

$$\xi = \frac{1}{3}log_{\alpha}\left(\alpha\beta\right) \tag{7}$$

$$\alpha = \frac{\rho_g}{\rho_l} \tag{8}$$

$$\beta = \frac{\mu_g}{\mu_l} \tag{9}$$

In this analysis, k_r represents the ratio of the radius of a stripped droplet to the wavelength of instability, and is assumed to be constant at 0.15 for all conditions [21]. k_t represents the the ratio of time it takes for mass to be stripped of the droplet to the time that it takes for a disturbance to grow, and is assumed to be 1 for all conditions.

In order to test the validity of this droplet stripping model, we compare the results obtained to experimental droplet breakup times. In this analysis, gas velocity behind the shock, u_{2g}, and gas density, ρ_{2g}, is determined from normal shock relations based on reported shock Mach numbers assuming ideal gas before and after the shock. Liquid density, ρ_l, liquid viscosity, μ_l, and gas viscosity, μ_g, is held constant before and after the shock, where these properties are obtained from NIST [22] at the base temperature and pressure of each fluid.

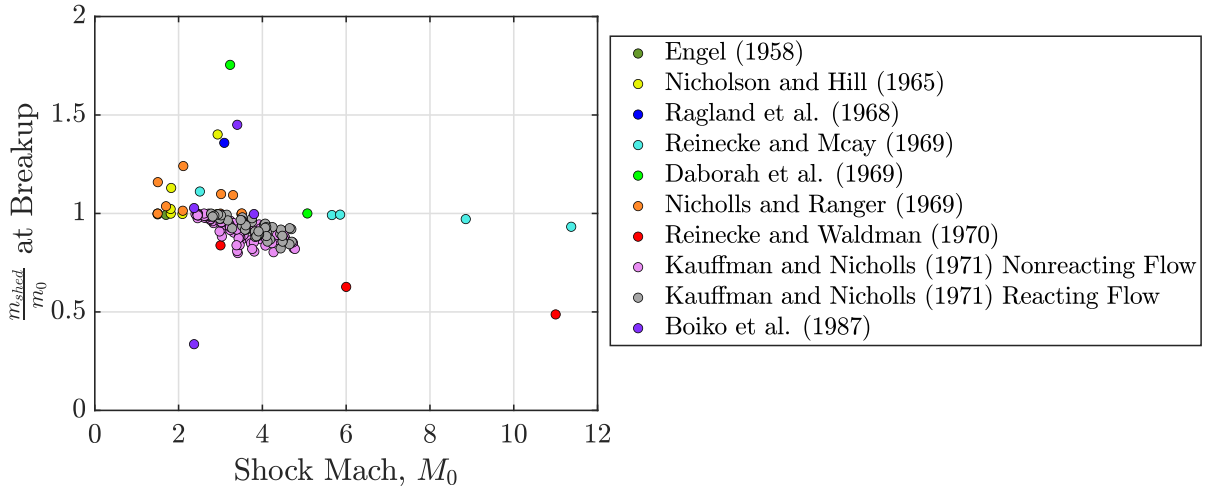

Fig. 2 Computed mass fraction of liquid shed from the parent drop at the experimentally determined breakup time vs the leading shock Mach number from compiled literature sources

If the droplet stripping analysis were to correlate perfectly to experimental data, then $\frac{m_{shed}}{m_0}$ at breakup would be 1; $\frac{m_{shed}}{m_0} < 1$ means that the effectiveness of droplet stripping is being underpredicted and $\frac{m_{shed}}{m_0} > 1$ means that the effectiveness of droplet stripping is being overpredicted. Figure 2 demonstrates that the droplet shedding analysis is approximately valid along the range of shock Mach numbers of interest. We note that there are a few test cases where the droplet stripping model tends to overpredict the rate of mass loss, but in the range of interest (Mach 4 - Mach 6), the droplet stripping model agrees quite well with experimental data. We note several caveats in attempting to model droplet behavior based on experimental data. First, reported breakup times were quantified based on visual observation and are thus a subjective measurement who's criteria may very based on experiment. Second, we expect the actual $\frac{m_{shed}}{m_0}$ at breakup to be slightly less than 1, because it has been observed [5] that the parent droplet may remain largely intact up until droplet breakup, when it will then rapidly disintegrate. This rapid disintegration at droplet breakup is likely

responsible for a large amount of heat release that triggers secondary blast waves observed in heterogeneous detonations [7]. The analysis of secondary blast waves is beyond the scope of the present analysis, but presents an important consideration for future work. Given these considerations, we find the droplet stripping analysis proposed by Girin to give reasonable correlation with experimental data across several literature sources for the range of conditions tested.

II. Droplet Modelling

A model has been constructed to inform the behavior of a droplet in a heterogeneous detonation flowfield. The purpose of this model is do discern trends in the time and length of the reaction zone as droplet size, base pressures, and mixtures are varied. A sketch of the flow being considered is shown in Fig. 3, and a flow chart of the model is

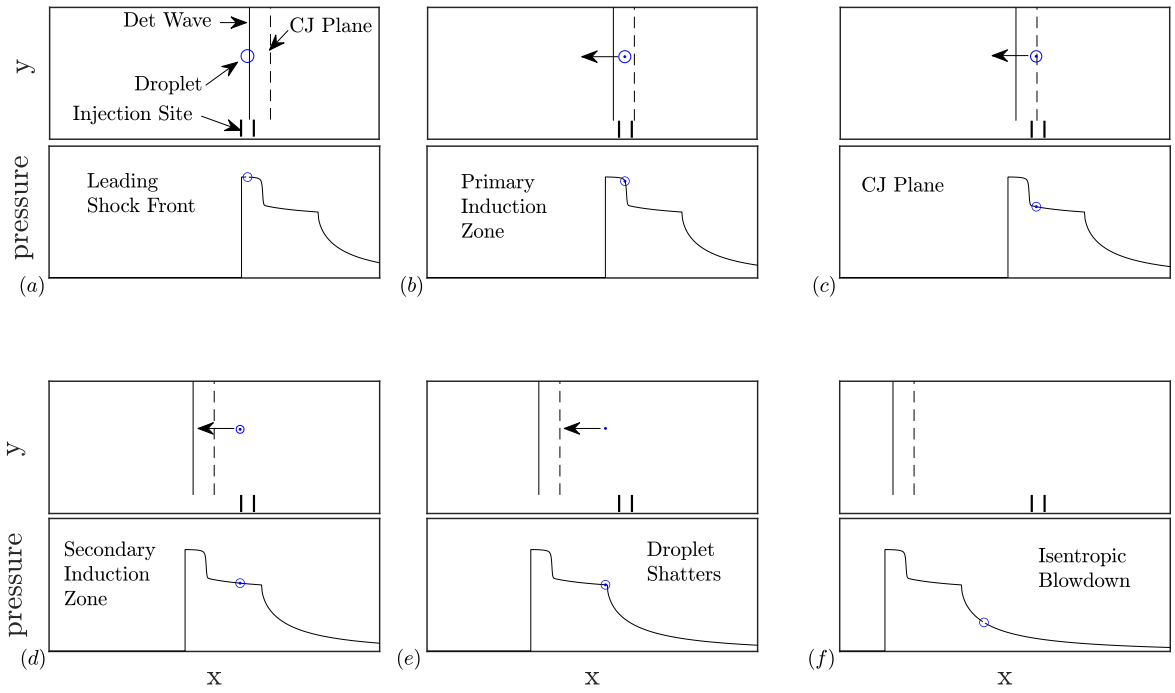

Fig. 3 Schematic showing stages of droplet shattering as a liquid droplet passes through a detonation wave. (a) The leading shock front hits the liquid droplet and the surrounding gas is pressurized. The droplet has no initial azimuthal velocity. (b) The droplet passes through the high-pressure region of the primary induction zone. The droplet begins to accelerate and shed mass due to the high dynamic pressure acting on the droplet from the surrounding gas. (c) The droplet hits the CJ plane and the surrounding gas pressure drops. (d) The parent droplet continues to accelerate and shed mass as it travels through the secondary induction zone. High pressure is still maintained as the mass shed from the droplet is burning.(e) The parent droplet completely shatters and any remaining mass from the parent droplet subsequently burns quickly. (f) The Droplet stops burning and the gas expands isentropically to the base pressure.

given in Fig. 4. The model considers the azimuthal behavior of gas/liquid reactants as they travel through the leading shock front and induction zone up to and past the Chapman-Jouguet (CJ) plane. Initially, reactants are injected at a base pressure, P_0, and global equivalence ratio, ϕ_{gl}, with no azimuthal velocity in the lab frame. It is assumed that the liquid is injected near its boiling temperature and the gas is injected at some prescribed temperature, T_{0g}. The prescribed droplet size is of the order of 1 mm, as this is the approximate size of an injected liquid jet column.

The reactants then pass through the leading shock front and travel through the region between the CJ plane and the leading shock front, which we name the primary induction zone. In the primary induction zone, the parent drop sheds mass and begins to burn, where the mechanism of atomization and droplet shedding is computed by Eq. (5). The droplet trajectory is tracked assuming that drag is the only force acting on the droplet, and the drag coefficient is taken to be constant at $c_d = 2.13$ for all conditions, selected from [4]. The equations of motion to describe the trajectory of the

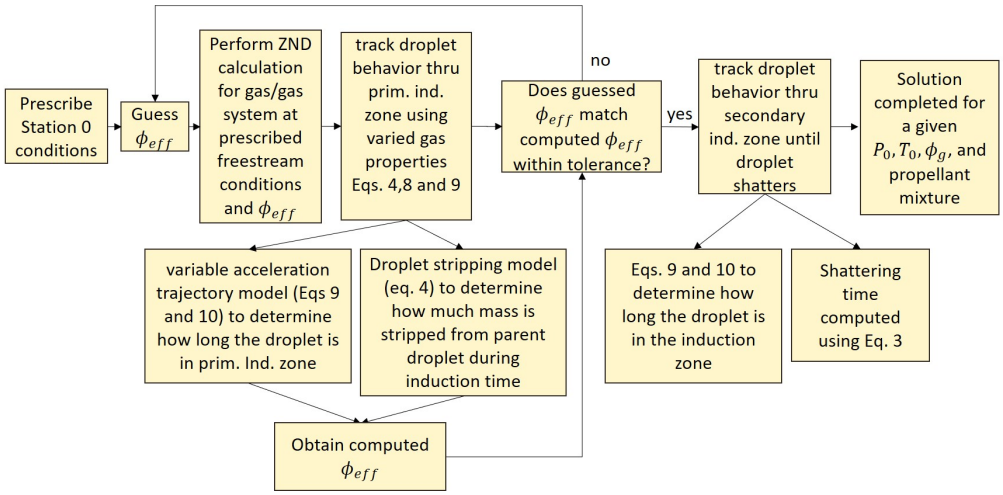

Fig. 4 Model Flow Chart

droplet are thus given by Eqs. (10-11).

$$\frac{du_l}{dt} = \frac{3}{4}\alpha\frac{c_d}{D}|u_g - u_l|(u_g - u_l) \tag{10}$$

$$\frac{dx_l}{dt} = u_l \tag{11}$$

It is desired to focus on the atomization and trajectory behavior of the droplet, and thus we uncouple the gas behavior from the droplet behavior. The gas properties in the induction zone are assumed to follow the zel'dovich-von Neumann-D*ö*ring (ZND) model, where the leading shock front is approximated as a nonreacting normal shock followed by a high-pressure reaction zone [23]. The Shock and Detonation Toolbox software with Cantera [24] was used to solve the ZND detonation structure.

As has been demonstrated in prior studies of heterogeneous detonations [17**?**] the parent droplet will not fully burn before it passes through the CJ plane. Thus, we define a region termed the secondary induction zone, which is the region in between the CJ plane and complete droplet shattering.

It is assumed that any portion of the droplet that is not shed within the primary induction zone does not contribute to the propagation of the detonation wave [25, 26]. The remaining portion of the droplet is assumed to be burned in the secondary induction zone until it reaches either the droplet shattering time computed by Eq. (2), or untill it reaches $\bar{m} = 0$ computed by Eq. (5). Thus, an effective equivalence ratio, ϕ_{eff} is defined, which is the equivalence ratio obtained by combusting all of the gas with only the portion of liquid shed in the primary induction zone. The ZND gas conditions are then obtained using $P_0, T_{0,g}$, and ϕ_{eff}. Three mixtures are considered for this study: $CH_4(g)/O_2(l)$, $O_2(l)/H_2(g)$, and $O_2(g)$/RP-2(l). The reaction mechanisms employed for each mixture are listed in Table 2.

Table 2 Reaction Mechanisms used for computing the ideal ZND detonation wave structure of each mixture

Mixture	Mechanism
O_2/CH_4	FFCM-1 [27]
O_2/H_2	Burke [28]
$O_2/RP2$	Hychem [29]

III. Results

The droplet shattering model described in Section II was run for a range of pressures and droplet sizes, where $\phi_g = 1$ and $T_{0g} = 298K$ were held constant. We will step through the results of the selected baseline case, which is a

$CH_4(g)/O_2(l)$ mixture at a base pressure of 10 atm and an initial droplet diameter of 1 mm. The computed trajectory of the droplet is shown in Fig. 5, along with the trajectory of the leading shock front, the CJ Plane, and the pathline of a parcel of gas that is injected at the same starting location as the droplet.

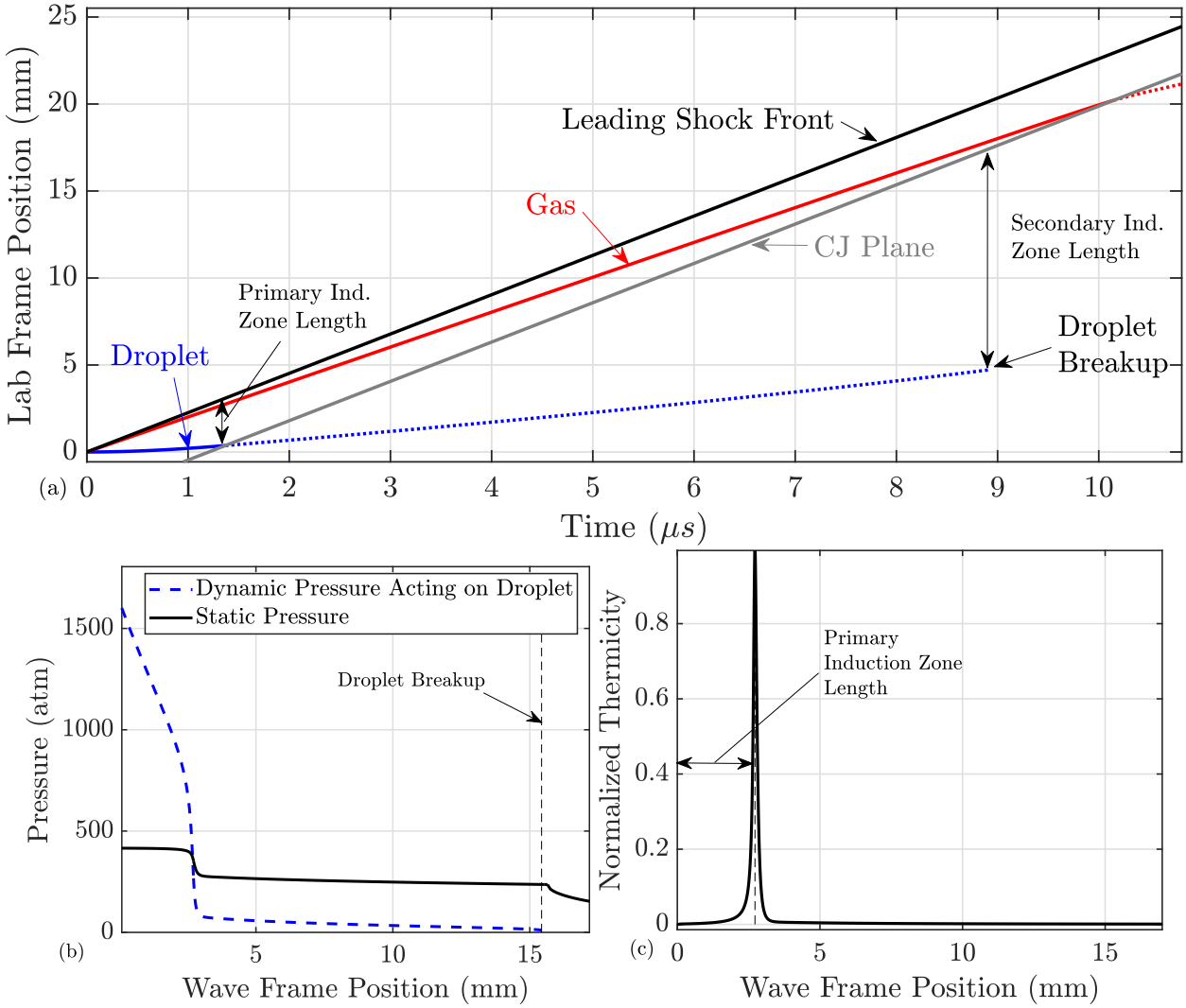

Fig. 5 (a) Computed trajectory of a 1mm O_2 droplet when hit by a 2260 m/s (Mach 5.85) detonation wave. Trajectory of the leading shock front, CJ Plane, and pathline of a parcel of gas is also shown.The solid line on the gas and liquid trajectories indicate that they are in the primary induction zone, and dotted lines indicate that they are in the secondary induction zone.(b) The static and dynamic pressure profile behind the leading shock front, where a wave-frame position = 0 is the location of the leading shock front.(c) The thermicity profile behind the leading shock front, which gives the primary induction zone length

.

Gaseous reactants impacted by the detonation wave will accelerate almost instantly to lab frame velocities that are close to the speed of the detonation wave. This induces a huge dynamic pressure on the droplet (Fig. 5(b)), which will cause the droplet to accelerate at a significantly slower rate than the gas. For these simulated conditions, the droplet will spend $1.37\mu s$ is the primary induction zone, and $7.60\mu s$ in the secondary induction zone before breaking up. During that time, the droplet will be pushed 4.82 mm away from it's original location. The gas on the other hand, gets pushed significantly further by the detonation wave. A parcel of gaseous reactant that starts in the same location as the droplet will travel 35.1 mm from it's original position in the time that it takes the droplet to break up. Because the leading shock front is able to accelerate the gas to higher velocities than the droplet, the gaseous reactants will spend longer in the

primary induction zone. This presents an interesting consideration for injector design, as it is likely that for a given fuel and ox element pair, the liquid component is reacting with gas from adjacent injector elements over the majority of it's burn.

The thermicity profile obtained from the ZND computation can be seen in Fig. 5(c). Shock heating induced by the leading shock front initiates exothermic reactions that raise the thermicity to it's peak, which is assumed to be the CJ plane. This metric is useful as it gives a consistent metric to measure the induction zone length.

A. Fuel Comparison

The differences in droplet behavior with fuel selection was studied for a 1 mm droplet at a base pressure of 10 atm. The resulting trajectories are shown in Fig. 6, and a comparison of key metrics from the results are shown in Table 3.

It is first noted that for all three mixtures, the overwhelming majority of the droplet lifetime is spent in the secondary induction zone. This is because, under the assumptions presented, the liquid will only need to shed a fraction of it's total mass (less than 30%) to propagate the detonation wave at the velocities listed in Table 3 (See Fig. 7(d)). This is not to say that the remaining portion of droplet mass burning in the secondary induction zone is undergoing "parasitic deflagration". Parasitic deflagration is low-pressure burning of propellant outside of the detonation heat-release zone and is associated with lowered performance in RDEs. The propellant being burned in the secondary induction zone is still being burned at pressures substantially higher than the base pressure and therefor will still have the benefit of higher thermal efficiency associated with burning at higher pressure. Thus, although it would be optimal to burn the majority of propellant in the primary induction zone, it is not implied that having the majority of propellant burn in the secondary induction zone would be a detriment to performance.

In comparing fluid properties, there is little variation in gas/liquid viscosity ratios behind the leading shock front (β_2) and thus we may consider viscosity to be uninfluential in differences observed between fuel selections. The density ratios (α_2), on the other hand, vary by several orders of magnitude between the three mixtures. This has a large influence on the trends observed as it impacts the dynamic pressure acting on the droplet (Fig. 7(a)). Because of the low density of hydrogen, the $O_2(l)/H_2(g)$ mixture has the lowest initial dynamic pressure acting on the droplet, despite having the highest gas velocity. This leads the O_2 droplet in the $O_2(l)/H_2(g)$ mixture to have the slowest acceleration, as well as the lowest rate of mass loss (See Fig. 7(d)). Because the rate of mass loss is the lowest, the reaction zone width widens, leading the $O_2(l)/H_2(g)$ mixture to have the longest primary induction length and the lowest shock mach number (M_0) of the three mixtures.

This leads to the question of physicality of this trend, which can be justified. The leading shock front can only travel as fast as the chemical reactions supporting it allow it to travel. If heat release increases the leading shock

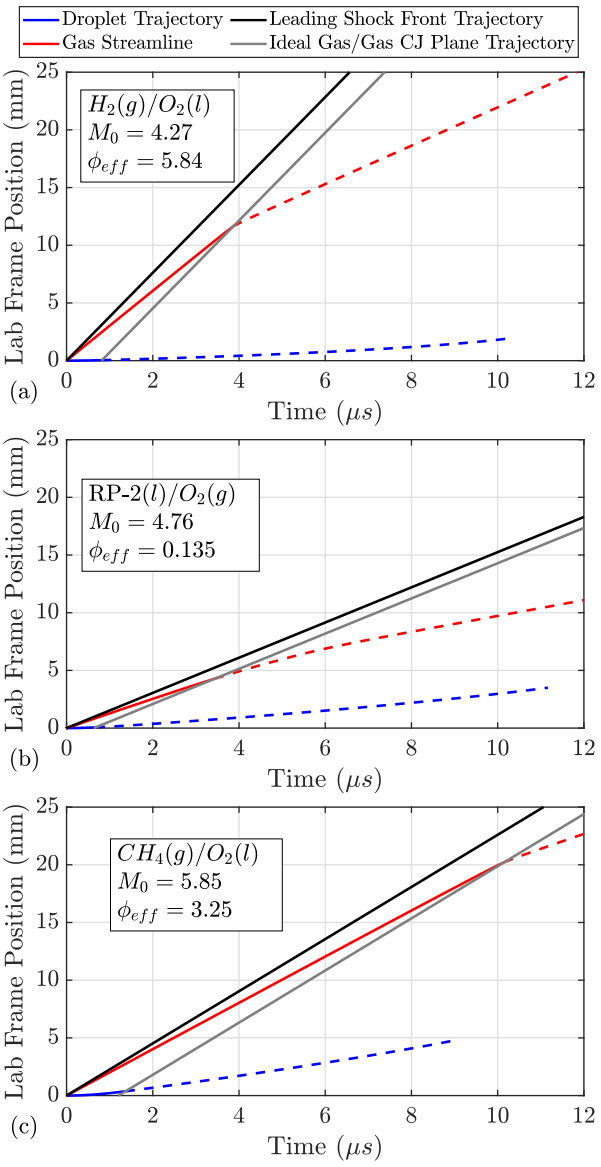

Fig. 6 Computed droplet trajectories of a 1 mm droplet at P_0 = 10 atm, T_{0g}= 298 K, and ϕ_g = 1 for (a) $H_2(g)/O_2(l)$, (b) $RP-2(l)/O_2(g)$, and (c) $CH_4(g)/O_2(l)$ mixtures. Solid lines on droplet and gas trajectories indicate the primary induction zone and dotted lines indicate the secondary induction zone.

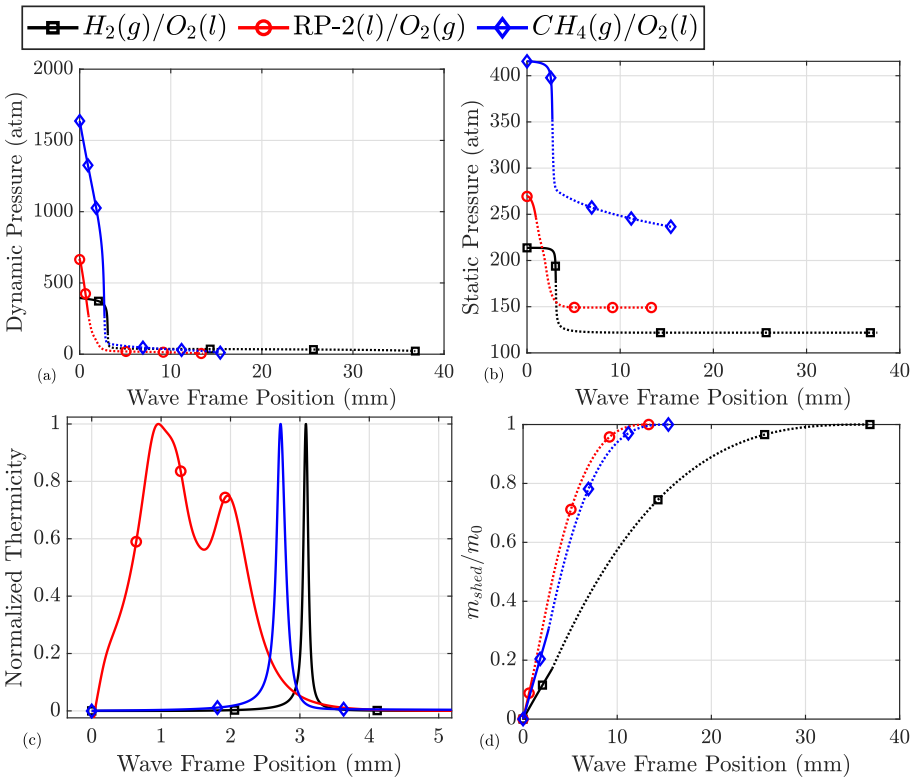

Fig. 7 Comparison of model results for a 1mm droplet at P_0=10 atm, T_{0g}=298 K, and ϕ_{gl} = 1 for the three different gas/liquid mixtures under consideration. (a) is the dynamic pressure acting on the droplet at the wave frame location of the droplet, (b) is the static pressure profile behind the leading shock front, (c) is the thermicity profile computed from ZND calculations at the converged ϕ_{eff}, and (d) is the normalized mass loss profile behind the leading shock front. In all charts, the solid lines are during the primary induction zone, and dashed lines are in the secondary induction zone until droplet breakup.

Table 3 Comparison of model results for a 1mm droplet at P_0=10 atm, T_0=298 K, and ϕ_{gl} = 1

Computed Value	$CH_4(g)/O_2(l)$	$O_2(g)$/RP-2(l)	$O_2(l)/H_2(g)$
M_0	5.85	4.76	4.27
Detonation Velocity (m/s)	2260	1400	3807
u_2 (m/s)	2011	1276	3027
β_2	0.28	0.35	0.26
α_2	.074	0.13	0.008
ϕ_{eff}	3.25	0.135	5.84
Primary Ind. Length (mm)	2.72	0.961	3.09
Secondary Ind. Length (mm)	12.8	12.6	34.5
Primary Ind. Time (μs)	1.37	0.674	0.821
Secondary Ind. Time (μs)	7.60	10.5	9.49
Total Droplet Distance Traveled (mm)	3.69	3.69	2.24

front speed faster than what the heat release can support,
the leading shock front will necessarily slow down because it has outrun the combustion process and can no longer be supported at that speed. Since it is established that droplet shattering is the rate-controlling mechanism of heat release,

the two prevalent factors that control the coupling of the heat release zone to the leading shock front are the dynamic pressure acting on the droplet and the soundspeed of the fluid medium.

Sound speed plays an important role here as fluids with higher sound speeds can support higher detonation velocities, which can permit the leading shock front to outrun the combustion process and fail. This behavior holds true for gas/gas detonations, but is a much more prevalent factor for heterogeneous detonations. The reason for this is because the gas has the ability to accelerate to near the velocity of the detonation wave, permitting a combustible mixture to remain present in the induction zone for a longer period of time, while the droplet accelerates slowly, and is thus in the primary induction zone for a much shorter period of time. We can see in Fig. 6, that the simple fact that hydrogen has a high sound speed leads to the $O_2(l)/H_2(g)$ mixture having the highest total induction length (38 mm), where the RP-2$(l)/O_2(g)$ and $CH_4(g)/O_2(l)$ mixtures have total induction lengths that are less than half this distance. This is an indication that an $O_2(l)/H_2(g)$ RDRE would be particularly difficult to sustain detonations because the leading shock front would be prone to decoupling from the wave.

It is widely accepted in literature based on experiment that heterogeneous detonations have substantially slower wavespeeds then gas/gas detonations [6–8]. A satisfactory explanation as to why this occurs is not present in the literature, and we believe that the present work is unique in illuminating a physical explanation to experimentally observed trends. Ragland et al. [6] argued that the deficit in propagation velocity was due to increased viscous and heat losses through the walls because of the widened reaction zone, claiming losses up to 20% of the enthalpy of reaction. We can argue that if this was the main source of velocity deficit, then gas/liquid RDREs would obtain horrendous performance. However, no experimental evidence exists in literature that there is a correlation between wavespeed and performance for RDEs. For the same reason, the argument of incomplete combustion as the sole cause of velocity deficit is also unsatisfactory.

We instead argue that heterogeneous detonations must have slower wavespeeds simply because the droplet is slow. If the detonation wave slows down then the droplet is allowed to stay in the primary induction zone for longer, which gives it more time to shatter, mix, and burn before being outrun by the leading shock front. This may permit us to hypothesize factors that may improve performance of RDREs. It is argued that we will have the best performance when the total induction length (primary + secondary) is minimized. This permits more of the propellant to be burned at high pressure, and there are several factors that can help with this. First, we can reduce droplet size. This would permit the droplet to accelerate faster, allowing it to stay in the primary induction zone longer. It also will reduce the time of droplet shattering, which will allow more of it to shatter in the primary induction zone. The second option is to select mixtures with lower sound speeds. This will permit the detonation wave to slow down without incomplete combustion.

Finally, it is interesting to note that the thermicity profile of an RP-2/O_2 detonation is substantially different from CH_4/O_2 and H_2/O_2 detonations. The ZND profile for CH_4/O_2 and H_2/O_2 reactions can be characterized as a long preiod of negligible heat release, followed by a narrow heat release zone. RP-2/O_2 on the other hand, begins the heat release process almost immediately after the leading shock front, and then has a much wider heat release zone. As a result, the pressure behind the leading shock front begins to drop immediately as the heat release acts to accelerate the gas away from the leading shock front. At this point it is unclear if this is advantageous or not, as increasing the heat release width does not necessarily change the droplet behavior at all.

B. Impact of Base Pressure

The impact of varying the base pressure was assessed, as this is an important consideration for pushing towards flight-relevant combustor conditions in RDREs. All experimental data in literature regarding droplet dynamics in heterogeneous detonations have considered base pressures of 1 atm or less, and thus this analysis will help to illuminate how changes in base pressure affect heterogeneous droplet behavior. The trajectory plots of a $CH_4(g)/O_2(l)$ mixture at base pressures of 1 atm, 10 atm, and 35 atm are shown in Fig. 8, and a comparison of relevant parameters for each case is shown in Table 4.

An interesting occurrence is observed when base pressure is varied. Increasing the base pressure will increase the rate of kinetics (Fig. 9(c)), and thus the low base pressure will have a wider primary induction zone length, despite having a higher M_0. Because the induction zone length is wider, more of the droplet can contribute to the wave propagation (Fig. 9 (d)) and the final ϕ_{eff} gets closer to unity as the base pressure is lowered. However, the dynamic pressure behind the wave scales with base pressure and thus the mechanism of droplet stripping and droplet acceleration is increased as base pressure, and thus α, increases. Ultimately, this leads to a closer coupling of the combustion with the leading shock front, as measured by the total induction length, as the base pressure increases.

Table 4 Comparison of model results for a 1mm O_2 droplet in CH_4 at T_0=298 K and ϕ_g = 1

Computed Value	$P_0 = 1atm$	$P_0 = 10atm$	$P_0 = 35atm$
M_0	6.30	5.85	5.67
Detonation Velocity (m/s)	2414	2260	2203
u_2 (m/s)	2161	2011	1956
β_2	0.24	0.28	0.29
α_2	.007	0.074	0.25
ϕ_{eff}	2.92	3.25	3.53
Primary Ind. Length (mm)	6.38	2.72	1.70
Secondary Ind. Length (mm)	29.0	12.8	8.08
Primary Ind. Time (μs)	2.73	1.37	1.01
Secondary Ind. Time (μs)	13.0	7.60	6.17
Total Droplet Distance Traveled (mm)	2.88	3.69	6.05

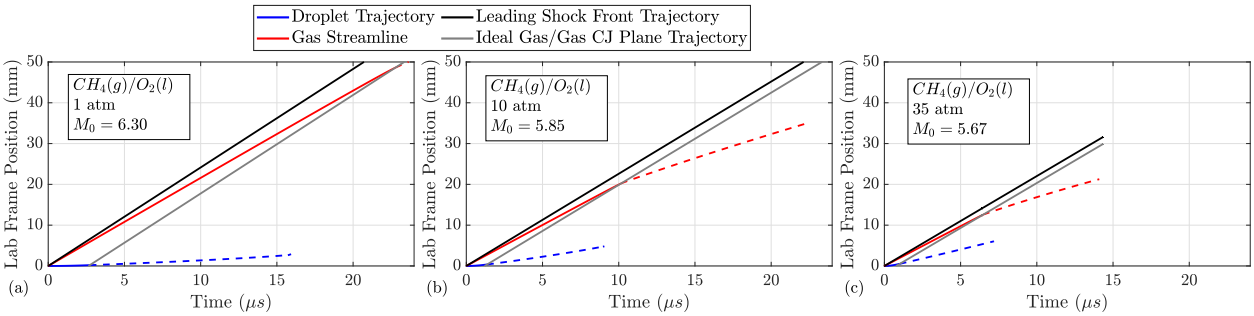

Fig. 8 Droplet trajectories of a 1 mm O_2 droplet in CH_4 at base pressures of (a) 1 atm (b) 10 atm and (c) 35 atm. $T_{0g} = 298K$ and $\phi_{gl} = 1$ for each case. Solid lines on droplet and gas trajectories indicate the primary induction zone and dotted lines indicate the secondary induction zone until droplet breakup.

C. Impact of Droplet Size

The impact of varying droplet size in a $CH_4(g)/O_2(l)$ mixture was assessed, where P_0 = 10 atm, T_{0g} = 298 K, ϕ_{gl} = 1 were held constant, and droplet sizes of 250 μm, 1000 μm, and 2000 μm were evaluated. As expected from literature, increasing the droplet size reduces the wavespeed and widens the total heat release zone. Necessarily, the larger droplet will have a substantially larger induction zone, because it has more mass to shed and will be a significant distance away from the leading shock front by the time it is done doing so. This is undesirable because it means that less of the droplet is burning in the high-pressure region behind the leading shock front (see Fig. 11(b)).

Unlike with pressure effects and fuel selection, the value of α changes by an insignificant amount between the different cases of droplet diameter. Thus, $\frac{m_{shed}}{m_0}$ only becomes dependent on the relative velocity between the liquid and the gas, and the value of t^*, which increases linearly with initial droplet diameter. If all properties were to remain the same except for droplet diameter, such that the gas profile experienced by the droplet remained consistent, then the rate of mass loss with respect to the original mass ($\frac{m_{shed}}{m_0}$) would increase with decreasing initial droplet diameter. Since a higher percentage of the total liquid mass is being shed in the primary induction zone, ϕ_{eff} is brought closer to unity and the detonation velocity subsequently increases. This leads to a higher dynamic pressure on the droplet, further permitting higher rates of mass shedding, and ultimately a faster, more closely-coupled detonation wave for the smaller droplet size.

Thus, as with traditional injectors, it is desirable to have small injector holes that can provide sufficient atomazition. One caveat to this is that more atomization will lead to more prevaporization due to the increased amount of surface area in potentially in contact with hot products. It is suspected that a small amount of prevaporization can be a good thing, as it may help with sustaining detonation wave propagation. However, too much prevaporation reduces the portion of reactants that are combusting in condensed phase, which will reduce the pressure ratio across the leading shock front.

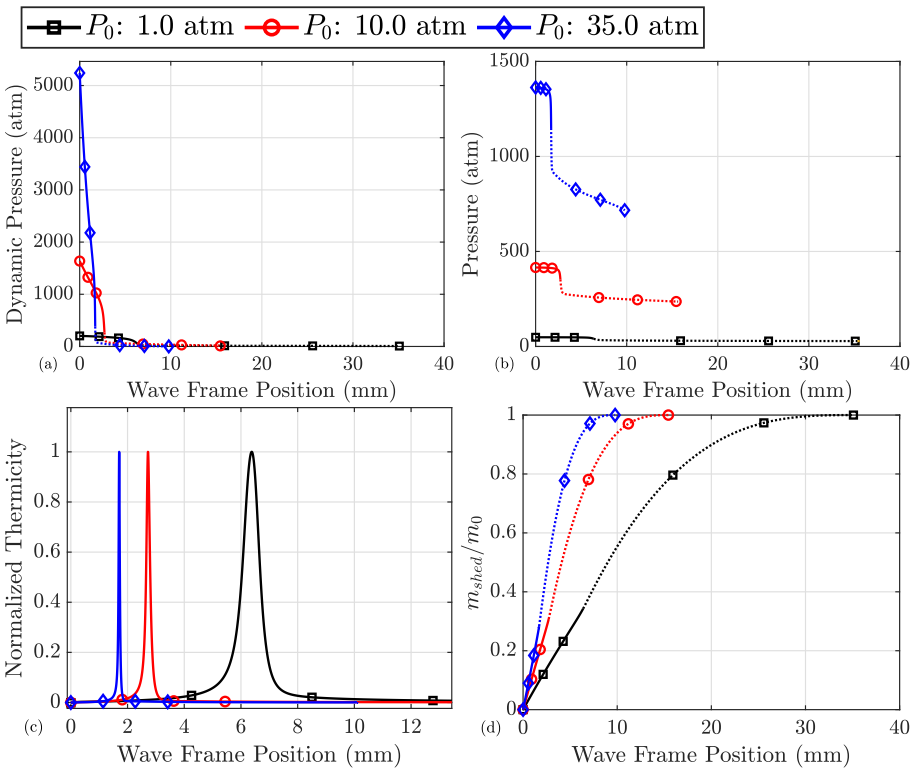

Fig. 9 Comparison of model results at varied base pressure for a 1mm O_2 droplet in CH_4 at T_{0g}=298 K and ϕ_{gl} = 1. (a) is the dynamic pressure acting on the droplet at the wave frame location of the droplet, (b) is the static pressure profile behind the leading shock front, (c) is the thermicity profile computed from ZND calculations at the converged ϕ_{eff}, and (d) is the normalized mass loss profile behind the leading shock front. In all charts, the solid lines are during the primary induction zone, and dashed lines are in the secondary induction zone until droplet breakup.

prevaporization is not addressed in the current manuscript, but is an area of future work.

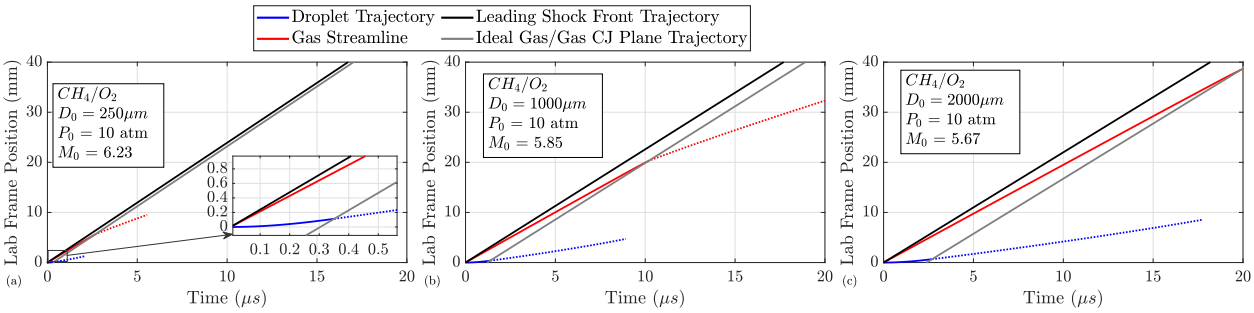

Fig. 10 Droplet trajectories of an O_2 droplet in CH_4 at P_0 = 10 atm, T_{0g} = 298 K, ϕ_{gl} = 1 and initial droplet diameters of (a) 250 μm (b) 1000 μm and (c) 2000 μm. Solid lines on droplet and gas trajectories indicate the primary induction zone and dotted lines indicate the secondary induction zone until droplet breakup.

D. Comparison to Experimental Data

It is finally desired to investigate how the trends observed apply to experimental RDRE combustors. For comparison to experiment, we will take conditions reported in the RDRE gox/kerosene test campaign of Lim et al. [30]. The selected condition of interest was a test case run at ϕ_{gl} = 1.72 with a chamber capillary tube attenuated pressure (CTAP)

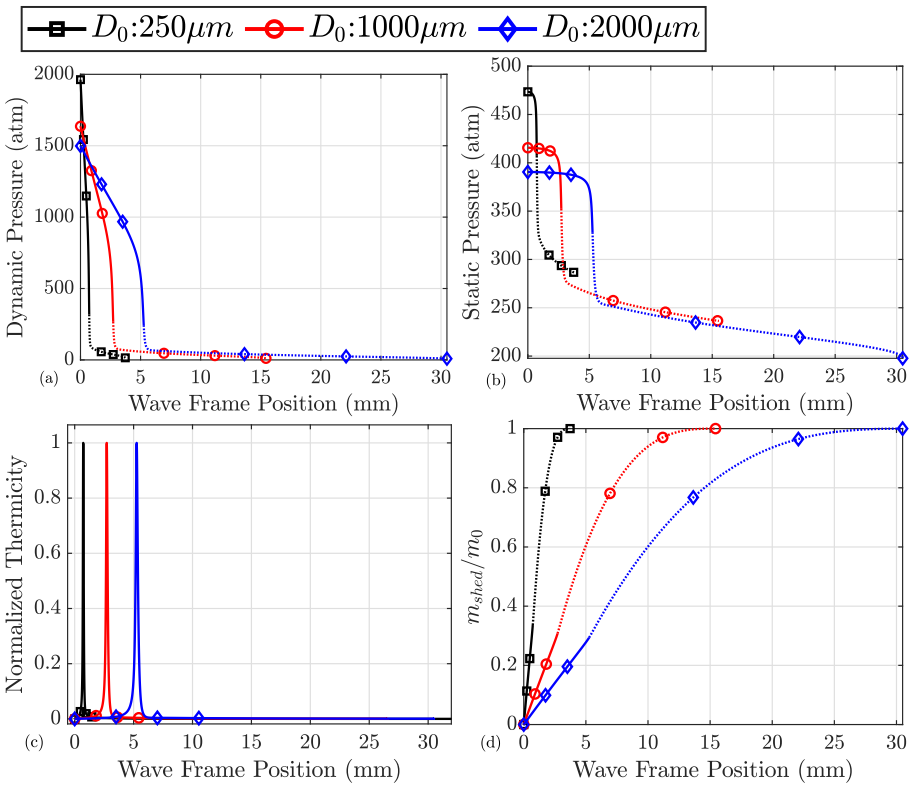

Fig. 11 Comparison of model results for an O_2 droplet of varied initial droplet diameters in CH_4 at T_0=298 K, P_0 = 10 atm and ϕ_g = 1.(a) is the dynamic pressure acting on the droplet at the wave frame location of the droplet, (b) is the static pressure profile behind the leading shock front, (c) is the thermicity profile computed from ZND calculations at the converged ϕ_{eff}, and (d) is the normalized mass loss profile behind the leading shock front. In all charts, the solid lines are during the primary induction zone, and dashed lines are in the secondary induction zone until droplet breakup.

Table 5 Comparison of model results for a 1mm O_2 droplet of varied initial droplet diameter in CH_4 at T_{0g}=298 K and ϕ_{gl} = 1

Computed Value	$D_0 = 250\mu m$	$D_0 = 1000\mu m$	$D_0 = 2000\mu m$
M_0	6.23	5.85	5.67
Detonation Velocity (m/s)	2391	2260	2200
u_2 (m/s)	2139	2011	1952
μ_2	0.29	0.28	0.28
ρ_2	0.078	0.074	0.072
ϕ_{eff}	2.98	3.25	3.40
Primary Ind. Length (mm)	0.726	2.72	5.26
Secondary Ind. Length (mm)	3.03	12.8	25.2
Primary Ind. Time (μs)	0.351	1.37	2.70
Secondary Ind. Time (μs)	1.76	7.60	15.6
Total Droplet Distance Traveled (mm)	1.32	4.82	9.83

of approximately 13.6 atm. The gox was heated with a preburner to approximately 400 K, and was injected through an annular slot that impinged with radial fuel holes at the gox injector throat. The fuel injector consisted of 120

evenly-spaced rectangular milled channels of 280 μm width and 150 μm depth. This gives an equivalent circular injector diameter of 233 μm. This test case generated four waves travelling at 1970 m/s, producing a wave spacing of 77 mm and a wave arrival time of 39.3 μs. Running the model for these conditions, the results shown in Fig. 12 are obtained.

The droplet burning analysis computed a detonation velocity of 1707 m/s (M_0 = 4.69), 10% lower than what was generated in experiment, and this is found to be fair agreement for the purpose of investigating the droplet behavior. Fig 12 shows the trajectory, where the to-scale injector elements are shown for reference. We can see that the droplet is larger than the primary induction zone length, and the droplet effectively does not move before the primary induction zone has completely passed the droplet. It is not until the secondary induction zone that the droplet begins to move by any appreciable amount, travelling a little over two injector diameters (.50 mm) before the droplet completely shatters. We note that the distance travelled by the droplet is only one fifth of the distance between adjacent injector elements, which have a center-to-center injector spacing of 2.58 mm. This is potentially advantageous for performance because the heat release can remain localized and does not span multiple injector elements.

Considering the disparity in length scales between the injector spacing and the droplet distance travelled, Fig. 12 implies that the detonation wave is operating as a series of discrete explosions that occur at or in between injector elements, as opposed to a continuous detonation event. One advantage of discrete, localized detonation events could be the reduction in parasitic deflagration, as hot combustion products are less likely to be dragged over freshly injected propellant after the passage of the leading shock front. Another potential advantage could be effective usage of secondary blast waves. We know that it is quite possible for the droplet, at some point during the secondary induction zone, to rapidly combust and form a blast wave that can travel upstream towards the leading shock front. This can cause the flow to unchoke and can help to accelerate the leading shock front. If the secondary blast wave occurs just prior to the leading shock front hitting the adjacent injector element, then this could create a pumping action which accelerates the leading shock front forward and increases the pressurization effect as the leading shock front compresses the fresh reactants of the adjacent injector. This creates strong motivation for further investigation into understanding secondary blast waves.

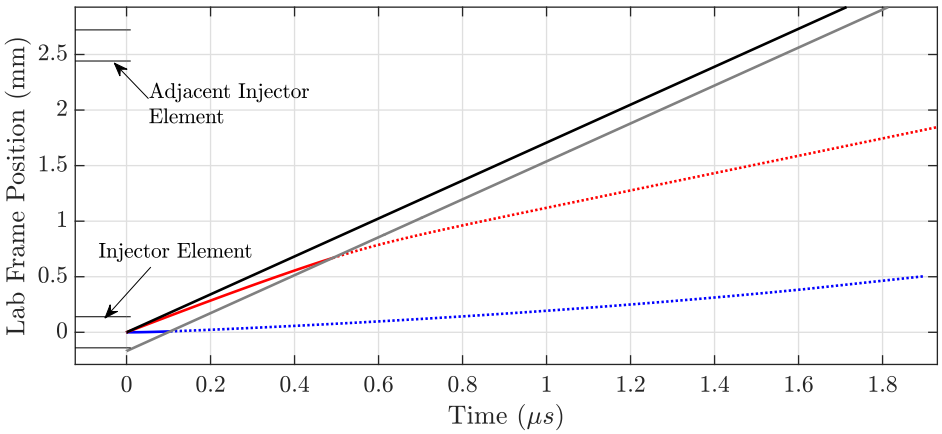

Fig. 12 Trajectory of a simulated RP-2 droplet in O_2 at representative conditions of a selected experimental RDRE test case from Lim et al.[30]. Horizontal lines show to-scale sizing of fuel injector orifice size and spacing compared to droplet and leading shock front trajectories.

IV. Conclusions

A droplet burning model has been constructed which utilizes experimental data to estimate droplet shattering times based on the dynamic pressure acting on the droplet, the initial droplet diameter, and the liquid density. A droplet shattering model is utilized, which estimates the rate of mass shed off the droplet based on viscous boundary layer instabilities at the free surface of the gas/liquid interface. This analysis was found to be in fair agreement with experimentally-determined droplet breakup times from several literature sources. The trajectory and rate of mass loss of the droplet was solved assuming that the droplet experienced surrounding gas equivalent to that of the reaction zone computed by a ZND calculation. This solution method was iterated until the amount of mass shed by the droplet in the primary induction zone provided the same amount of heat release needed to propel the detonation at a speed sufficient to produce the correct amount of dynamic pressure to shatter the droplet at this rate. This solution method for analyzing

the droplet shattering behavior in a detonation wave permits us to identify useful trends and key metrics that may affect heterogeneous RDRE performance, while circumventing detailed numerical solutions.

It is desired to understand the implications of the trends discussed with respect to their impact RDRE performance. Without an in-depth derivation, we can infer that a close coupling of the heat release with the leading shock front is desirable for improving performance, as a closely-coupled detonation will increase the amount of propellant burned at high pressure, leading to a more efficient combustion process. Ultimately, the best metric for this is the total induction length, as this measures how far away the leading shock front is from the droplet mass by the time breakup occurs.

Increasing the droplet size significantly increases the induction length, as there is simply more mass to shed. Increasing base pressure substantially reduces the induction zone length, because increasing the base pressure will increase the dynamic pressure behind the wave, allowing the droplet to have a higher acceleration and rate of mass loss.

While varying the droplet diameter and base pressure have rather straightforward consequences on the induction length, the choice of propellant mixture is more complex, and its influence can be broken down into two factors: the chemical kinetics and the sound speed. Since the droplet breakup is the rate controlling mechanism of combustion, it is argued that kinetics play a more minor role in the wave dynamics of heterogeneous detonations than they would for gas/gas systems. Thus, the primary factor influencing the induction zone length is the reactant sound speed. In can be inferred that it is desired to have a lower reactant sound speed for close coupling of the heat release zone to the leading shock front. Finally, the droplet shattering analysis was applied to a gox/kerosene experimental RDRE test condition from Lim et al. [30]. It is estimated that because of the small fuel injection orifices used, the heat-release zone behind the detonation wave likely occurs quite local to the injection orifice, with potentially large gaps of little heat release in between injection orifices.

V. Acknowledgments

The authors would like to acknowledge AFOSR Program officers Dr. Chiping Li and Dr. Eric Paulson (contract FA9300-20-C-2001) in this study. Additionally the authors would like to thank Dr. Swanand Sardeshmukh and Dr. Jenna Humble for their expertise.

References

[1] Humble, J., and Heister, S. D., "Heterogeneous Detonation Physics as Applied to High Pressure Rotating Detonation Engines," *AIAA Scitech 2021 Forum*, 2021, p. 1027.

[2] Engel, O., "Fragmentation of waterdrops in the zone behind an air shock," *Journal of Research of the National Bureau of Standards*, Vol. 60, No. 3, 1958, p. 245. https://doi.org/10.6028/jres.060.029, URL https://nvlpubs.nist.gov/nistpubs/jres/60/jresv60n3p245_A1b.pdf.

[3] Nicholson, and Hill, "RAIN ERDSIDN DN SPIKE-PRDTECTED SUPERSONIC RADDMES," 1965.

[4] Reinecke, and Mcay, "EXPERIMENTS ON WATER DROP BREAKUP BEHIND MACH 3 TO 12 SHOCKS," , 1969.

[5] Reinecke, W., and Waldman, G., "A study of drop breakup behind strong shocks with applications to flight," Tech. rep., AVCO SYSTEMS DIV WILMINGTON MA, 1970.

[6] Ragland, K. W., "Observed Structure of Spray Detonations," *Physics of Fluids*, Vol. 11, No. 11, 1968, p. 2377. https://doi.org/10.1063/1.1691827, URL https://aip.scitation.org/doi/10.1063/1.1691827.

[7] Dabora, E., Ragland, K., and Nicholls, J., "Drop-size effects in spray detonations," *Symposium (International) on Combustion*, Vol. 12, No. 1, 1969, pp. 19–26. https://doi.org/10.1016/S0082-0784(69)80388-7, URL https://linkinghub.elsevier.com/retrieve/pii/S0082078469803887.

[8] Nicholls, J., and Ranger, A., "Aerodynamic shattering of liquid drops." *Aiaa Journal*, Vol. 7, No. 2, 1969, pp. 285–290.

[9] Kauffman, C. W., and Nicholls, J. A., "Shock-wave ignition of liquid fuel drops," *AIAA Journal*, Vol. 9, No. 5, 1971, pp. 880–885. https://doi.org/10.2514/3.6290, URL https://arc.aiaa.org/doi/10.2514/3.6290.

[10] Boiko, V. M., Papyrin, A. N., and Poplavskii, S. V., "Dynamics of droplet breakup in shock waves," *Journal of Applied Mechanics and Technical Physics*, Vol. 28, No. 2, 1987, pp. 263–269. https://doi.org/10.1007/BF00918731, URL http://link.springer.com/10.1007/BF00918731.

[11] Cramer, F. B., "The onset of detonation in a droplet combustion field," *Symposium (International) on Combustion*, Vol. 9, Elsevier, 1963, pp. 482–487.

[12] Bowen, J. R., Ragland, K. W., Steffes, F. J., and Loflin, T. G., "Heterogeneous detonation supported by fuel fogs or films," *Symposium (International) on Combustion*, Vol. 13, No. 1, 1971, pp. 1131–1139. https://doi.org/10.1016/S0082-0784(71)80110-8, URL https://www.sciencedirect.com/science/article/pii/S0082078471801108.

[13] Ragland, K., Dabora, E., and Nicholls, J., "A study of heterogeneous detonations," *3rd and 4th Aerospace Sciences Meeting*, American Institute of Aeronautics and Astronautics, New York,NY,U.S.A., 1966. https://doi.org/10.2514/6.1966-109, URL http://arc.aiaa.org/doi/10.2514/6.1966-109.

[14] Bar-Or, R., Sichel, M., and Nicholls, J. A., "The propagation of cylindrical detonations in monodisperse sprays," *Symposium (International) on Combustion*, Vol. 18, No. 1, 1981, pp. 1599–1606. https://doi.org/10.1016/S0082-0784(81)80163-4, URL https://www.sciencedirect.com/science/article/pii/S0082078481801634.

[15] Bar-Or, R., Sichel, M., and Nicholls, J. A., "The reaction zone structure of cylindrical detonations in monodisperse sprays," *Symposium (International) on Combustion*, Vol. 19, No. 1, 1982, pp. 665–673. https://doi.org/10.1016/S0082-0784(82)80241-5, URL https://www.sciencedirect.com/science/article/pii/S0082078482802415.

[16] Cheatham, S., and Kailasanath, K., "Numerical modelling of liquid-fuelled detonations in tubes," *Combustion Theory and Modelling*, Vol. 9, No. 1, 2005, pp. 23–48.

[17] Eidelman, S., and Burcat, A., "Evolution of a detonation wave in a cloud of fuel droplets. I-Influence of igniting explosion," *AIAA Journal*, Vol. 18, No. 9, 1980, pp. 1103–1109.

[18] Borisov, A. A., Gel'fand, B. E., Gubin, S. A., Kogarko, S. M., and Podgrebenkov, A. L., "Detonation reaction zone in two-phase mixtures," *Combustion, Explosion, and Shock Waves*, Vol. 6, No. 3, 1970, pp. 327–336. https://doi.org/10.1007/BF00742508, URL http://link.springer.com/10.1007/BF00742508.

[19] Borisov, A. A., Kogarko, S. M., and Lyubimov, A. V., "Sliding of detonation and shock waves over liquid surfaces," *Combustion, Explosion, and Shock Waves*, Vol. 1, No. 4, 1967, pp. 19–23. https://doi.org/10.1007/BF00748807, URL http://link.springer.com/10.1007/BF00748807.

[20] Girin, A. G., "Hydrodynamic instability and regimes of fragmentation of drops," *Journal of engineering physics*, Vol. 48, No. 5, 1985, pp. 560–564. https://doi.org/10.1007/BF01840722, URL https://doi.org/10.1007/BF01840722.

[21] Girin, A. G., "Equations of the kinetics of droplet fragmentation in a high-speed gas flow," *Journal of Engineering Physics and Thermophysics*, Vol. 84, No. 2, 2011, pp. 262–269. https://doi.org/10.1007/s10891-011-0468-x, URL http://link.springer.com/10.1007/s10891-011-0468-x.

[22] Lemmon, E. W., McLinden, M. O., and Friend, D. G., *Thermophysical properties of fluid systems, NIST chemistry webbook, NIST standard reference database.*, 69, National Institute of Standards and Technology, Gaithersburg MD, 20899, 2016.

[23] Lee, J. H., *The detonation phenomenon*, 2008.

[24] Browne, S., Ziegler, J., and Shepherd, J. E., "Numerical Solution Methods for Shock and Detonation Jump Conditions," , 2004.

[25] Gubin, S., and Sichel, M., "Calculation of the detonation velocity of a mixture of liquid fuel droplets and a gaseous oxidizer," *Combustion Science and Technology*, Vol. 17, No. 3-4, 1977, pp. 109–117.

[26] Pierce, T., and Nicholls, J., "Time variation in the reaction-zone structure of two-phase spray detonations," *Symposium (International) on Combustion*, Vol. 14, Elsevier, 1973, pp. 1277–1284.

[27] Smith, G. P., Tao, Y., and Wang, H., "Foundational Fuel Chemistry Model Version 1.0 (FFCM-1)," , 2016. URL http://web.stanford.edu/group/haiwanglab/FFCM-1/index.html.

[28] Burke, M., Chaos, M., Ju, Y., Dryer, F., and Klippenstein, S., "Comprehensive H2/O2 Kinetic Model for High-Pressure Combustion," , 2011.

[29] Xu, R., Wang, K., Banerjee, S., Shao, J., Parise, T., Zhu, Y., Wang, S., Movaghar, A., Lee, D., Zhao, R., Han, X., Gao, Y., Lu, T., Brezinsky, K., Egolfopoulos, F., Davidson, D., Hanson, R., Bowman, C., and Wang, H., "A physics-based approach to modeling real-fuel combustion chemistry - II. Reaction kinetic models of jet and rocket fuels," , 2018.

[30] Lim, D., Humble, J., and Heister, S., "Experimental Testing of an RP-2-GOX Rotating Detonation Rocket Engine," 2020. https://doi.org/10.2514/6.2020-0195.